Experimental Studies on Steady-state Oil Flows through Restrictors

By

Seiichi WASHIO*, Tadataka KONISHI** and Norihiko HIGASHIDE***

Abstract

When orifices and nozlzes are used in oil hydraulic lines, some of their characteristics come out more distinctly, owing to a high oil viscosity, than for less viscous fluids like water and gas. Taking advantgae of this fact, this paper intends to contribute toward the study of steady-state constriction flows, by conducting a few elementary measurements of oil flows through restrictors. In the first place pressures are measured on a pipe wall before and after a circular orifice. The rseults force the classical picture of an orifice flow to be modified. That is, the pressure begins to decrease from several pipe-diameters upstream from the orifice, instead of sightly increasing toward the orifice as has conventionally been imagined. Furthermore, in the downstream region, the pressure recovery suddenly disappears for Reynolds numbers below a certain critical value. Secondly, the mouth area - pressure drop - flow rate relations are properly measured for a poppet-type restrictor. It turns out that a linear loss as well as a non-linear loss plays an important role in a constriction oil flow around a poppet. The results are further used to predict the static performances of the poppet valve when it works as a relief valve for an ordinary purpose.

1. Introduction

The non-linear loss problem of steady flows through orifices and nozzles has been considered in hydraulics, where the following empiric formula represents their characteristics. That is, when the pressure drop across, and the flow rate through an orifice are denoted by Δp and q, respectively, the relation between them is given for incompressible fluids by

$$q = \frac{C_f A}{\sqrt{1-m^2}} \sqrt{\frac{2\Delta p}{\rho}} \tag{1}$$

where ρ is the fluid density, A the cross-sectional area of the orifice, and m the ratio of A to the cross-sectional area of the channel. Moreover, C_f is called a

---

* Department of Precision Mechanics
** Department of Applied Mechanics, Okayama University
*** Nipphon Sheet Glass Co. Ltd., Japan

'discharge coefficient', and experimentally determined as a function of the orifice geometry, m and the Reynolds number.

Since orifices and nozzles have traditionally been applied to measure rates of water and air flows in channels, the major concern about them has been turned to precisely estimating the discharge coefficient C_f[1)-4)]. However, fundamental knowledge about the very structure of a constriction flow remains not only scanty but also incomplete at present. Speaking of a pressure distribution across an orifice, for example, the following model is accepted as its true picture[5)]. That is, in the upstream proximity, the reduction of axial velocity components toward an orifice wall causes a slight increase of the pipe wall pressure. Then, the flow is throttled and the static pressure is converted into kinetic energy. Though most of the kinetic energy dissipates in the downstream jet turbulence, there always occurs some static pressure recovery within 4 to 6 pipe-diameters away from the orifice. Strangely enough, however, this familiar picture of an orifice-in-a-pipe flow has not been sufficiently verified through experiments.

Now, our primary concern lies in restricted flows in 'oil' hydraulic lines. Hence, this paper intends to contribute to the study on a steady-state constriction flow through a restrictor by experiments with the use of oil as a fluid. We first measure the pressure distributions along a pipe wall upstream and downstream from an orifice, and examine the validity of the conventional model for them.

Pressures and flow rates are often controlled in oil hydraulic systems by varying the opening area of a restrictor mouth. Therefore, exact knowledge about the relations among the opening area A, pressure drop Δp and flow rate q of a restrictor are required for a good system design. It seems, however, that most designers simply rely on an apriori assumption that Eq. (1) can well predict the relations, and so, dispense with any experimental confirmation.

This paper is also concernes with this problem, and takes up a poppet-type pressure control valve as a typical variable area restrictor. Then, the opening area-pressure drop-flow rate relations for the poppet valve are precisely measured. An empiric formula is sought to estimate the results, and then compared with the conventional one like Eq. (1). This formula further helps predict the actual performances of the poppet valve when it is ordinarily used as a pressure regulating element.

2. Pressure distributions in orifice flows

2.1 Experimental apparatus

We make such a cylindrical channel with a narrow circular hole at the end, as is illustrated in Fig. 1. Letting oil flow in opposite directions, we can separately
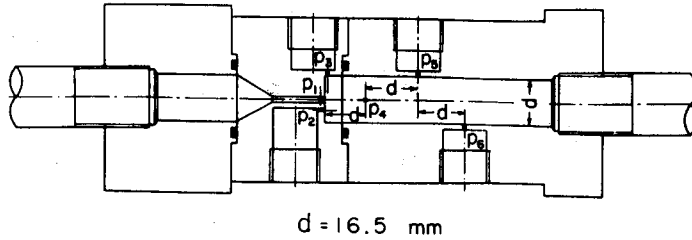
d = 16.5 mm

Fig. 1. Channel geometry for orifice flow measurements.

generate the same two flows, as are seen upstream and downstream from a circular orifice in a pipe. Tow kinds of hole diameters $d_0 = 1$ and 2 mm are employed, whereas the channel has a constant diameter $d = 16.5$ mm. As shown in Fig. 1, pressures are measured at 6 separate holes of 0.5 mm diameter on the wall. Among them, four, ($p_3 \sim p_6$), are placed along the channel wall in the axial direction in such a way as to keep p_3 1 mm away from the end wall, and all at every diameter d. The rest are on the end wall, 3.3 mm from the center (p_2) and on the nozzle wall, 1.5 mm inside the mouth (p_1). Fluids used in the test are Turbine Oil 140# ($\nu = 1.49$ cm²/s at 20°C) and Spindle Oil 60# ($\nu = 0.23$ cm²/s at 20°C). Semiconductor pickups and a thermistor measure the pressures and the oil temperature, respectively. Moreover, a platform scale and stopwatch are useful for weighing the steady flow rates of the oils.

2.2 Upstream convergent flow

Pressures p_1 to p_5, measured for steady flows contracting from the broad channel toward the small tube, are plotted in Fig. 2, outlining the general shapes of pressure distributions. Reynolds numbers, referring to the nozzle diameter, i.e.,

$$Re = q \bigg/ \left(\frac{\pi}{4} \nu d_0 \right)$$

for each measurement, are indicated on the right side of the p_5 points together with the flow rates in parentheses.

The results are interesting. Contrary to expectations, the pressure along a pipe wall decreases greatly for a large Re, toward the orifice, which is known from the pressure drops between p_4 and p_5 in particular. The starting point of such pressure drops seems to be more than two pipe-diameters upstream from the orifice. This is a peculiar phenomenon which has not been reported, as far as the authors know. Moreover, this result contradicts the conventional assertion that the pressure should slightly increase toward an orifice in its upstream vicinity.

Now, we look at the intriguing pressure fall from p_5 to p_4 from another point of view. Following the tradiational expression in hydraulics, we introduce the loss coefficient ζ_{45} as
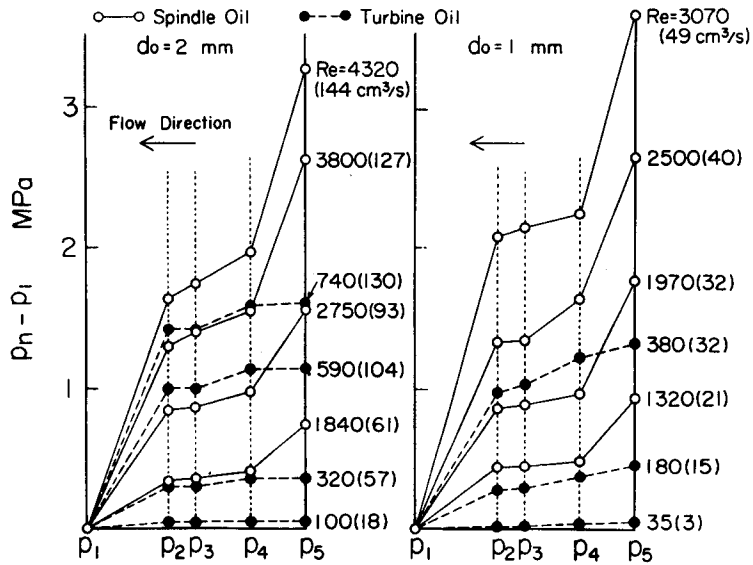
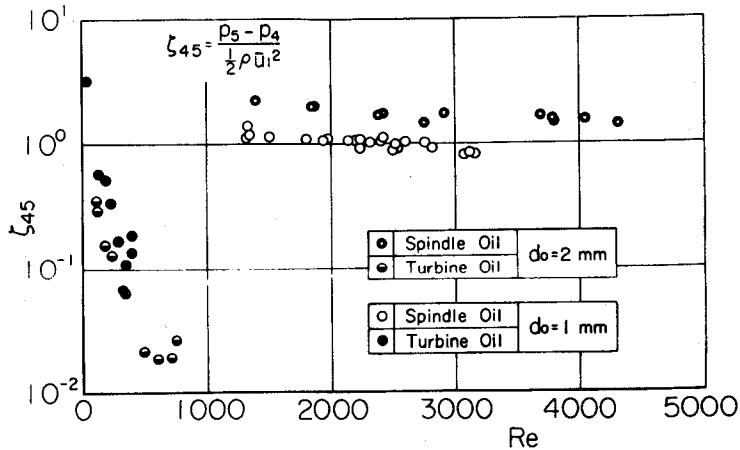Fig. 2.   Pressure distributions in upstream convergent flow.

Fig. 3.   Loss coefficient ζ_{45} for upstream local pressure drop p_5-p_4.

$$p_5-p_4 = \frac{1}{2}\zeta_{45}\rho\bar{u}_1^2 \tag{2}$$

where $\bar{u}_1$ is the average velocity in the nozzle tube.   Plotting ζ_{45}, calculated from the the above-obtained data versus Re, yields Fig. 3.

Apparently, the values of ζ_{45} are split into two different groups, below and above $Re=1000$.   This result suggests that an upstream convergent flow changes its nature substantially at a certain critical value of Re, which recalls the classical

experiments by Stanton and Pannel for laminar and turbulent losses in pipe flows. However, at present we do not know whether this sudden change depends on **Re** alone, or on other factors as well.

Next, we direct our attention to the total pressure loss between sections 5 and 1, instead of $p_5 - p_4$, and estimate it with the similar loss coefficient ζ_5 defined by

$$\left(p + \frac{1}{2}\rho\bar{u}^2\right)_5 - \left(p + \frac{1}{2}\rho\bar{u}^2\right)_1 = \frac{1}{2}\zeta_5\rho\bar{u}_1^2 \tag{3}$$

The result is shown in Fig. 4. In this case, the difference between the two groups is much smaller than in Fig. 3. The fact that some gaps still remain around **Re**=1000 probably means that the pressure hloe 5 is too far from the orifice wall to get a loss coefficient independent of **Re**. So, choosing hole 3 in place of 5, and plotting ζ_3 defined by
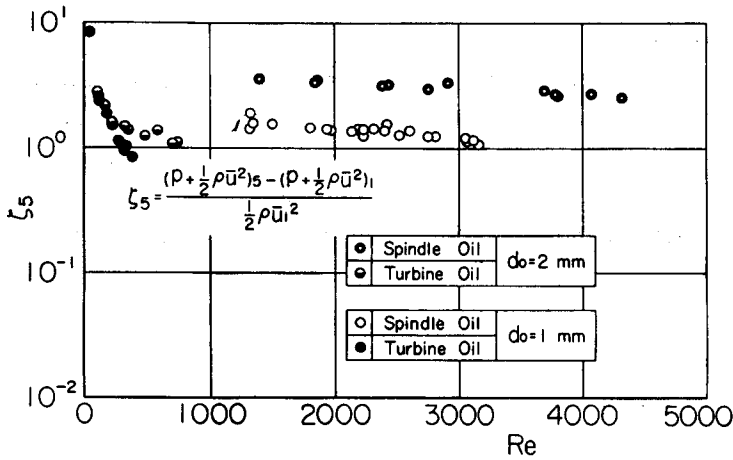

Fig. 4. Loss coefficient ζ_5 for upstream total pressure drop $p_5 - p_1$.

$$p_3 - \left(p + \frac{1}{2}\rho\bar{u}^2\right)_1 = \frac{1}{2}\zeta_3\rho\bar{u}_1^2 \tag{4}$$

we have Fig. 5. Though the values for $d_0 = 1$ mm are a little scattered, the discontinuities seem to have disappeared in Fig. 5, especially for $d_0 = 2$ mm. Since ζ_3 is almost equivalent to C_f in Eq. (1), Fig. 5 shows that the discharge coefficients will hardly help reveal the peculiar phenomenon which is found above. Moreover, when circular orifices are applied for measuring the flow rates in the oil lines, the pressure holes across an orifice must be placed as close to the orifice wall as possible, in order to avoid the effects of a temperature change.
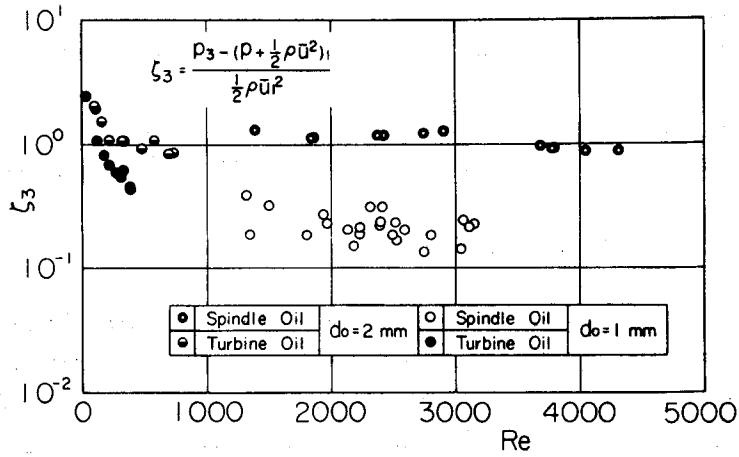
Fig. 5.   Loss coefficient ζ_3 for upstream pressure drop along orifice wall.

2.3   Downstream divergent flow

Pressures, flow rates and temperatures are similarly measured here as Spindle Oil jets out from the nozlze into the channel.   Figure 6 demonstrates the downstream pressure distributions with data examples of p_3 to p_6 and their corresponding Reynolds numbers.   These results generally agree with the conventional picture of pressure distribution downstream from an orifice.   Namely, along a pipe wall in
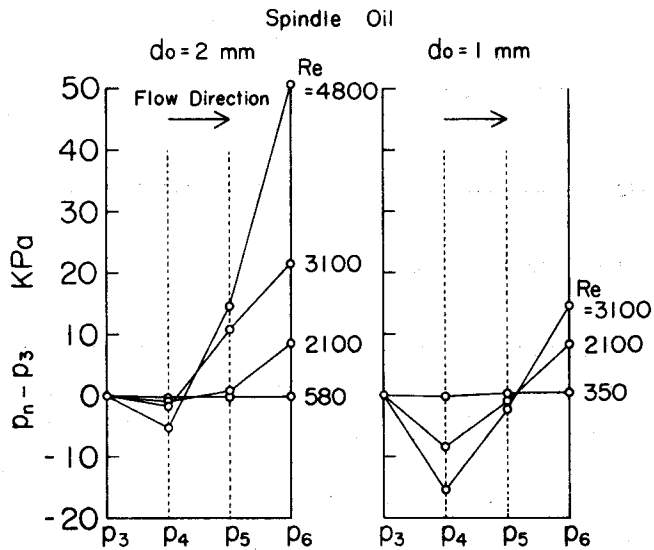

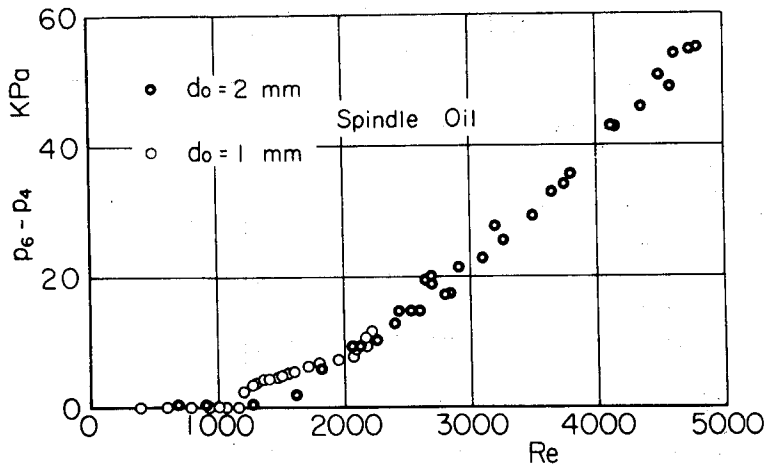Fig. 6.   Pressure distributions in downstream jet flow.

Fig. 7.   Local pressure recovery $p_6 - p_4$ in downstream jet flow.

the axial direction, the static pressure first goes down slightly, due to the contraction of jet flow, and then makes a recovery.   It is interesting, however, that neither the contraction drop nor the recovery of pressure seems to exist for a small Re. In order to make this point clear, we plot $p_6 - p_4$ versus Re in Fig. 7.   The result shows that the pressure recovery $p_6 - p_4$ disappears rather suddenly below $Re =$ 1300.   This is another intriguing phenomenon which as yet has not been reported up to the present time.   Although it is conceived that the downstream orifice flow changes its nature at a certain critical Re, we cannot explain now how and why it occurs.

2.4   Hypothetical picture of pressure distribution

The experimental data obtained here are quite limited.   Nevertheless, we think it is useful to draw a hypothetical picture of the profile of the pressure drop and recovery in an orifice-in-a-pipe flow with all the above results.   The whole picture is illustrated in Fig. 8.   The substantial difference of this model from conventional ones lies in what we call the 'constriction loss $I = p_I$ in the upstream region.   Moreover, the pressure recovery p_V in the downstream flow is supposed to disappear when Re becomes smaller than a critical value.   The 'laminar flow recovery' is characteristic of high viscous oil lines.   Although in Fig. 8 the downstream laminar flow begins just where the pressure recovery hits the maximum, we have no evidence that it actually holds true.   For convenience sake, we define the flow domain from the upstream end of a laminar flow to its downstream start as the 'orifice flow region'.
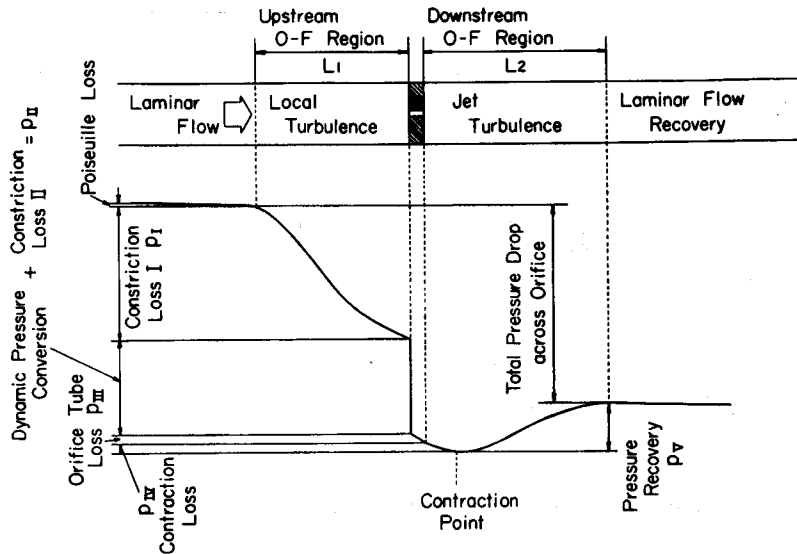
Fig. 8.   Hypothetical model of pressure distribution across an orifice in a pipe.

3. Characteristics of poppet-type restrictor

It is commonly utilized for the purpose of controlling pressures and flows in oil hydraulic systems to vary an opening flow area of a restrictor.   Then, most designers rely on Eq. (1), and expediently assume that the discharge coefficient C_f is independent of the opening area A, when they try to predict the behaviors of such restrictors.   However, we believe that that standpoint requires experimental checks before being accepted as true.   Here we take up a poppet-type restrictor as a typical example, and find how its loss coefficient is related with the opening area.

3.1 Experimental device and method

An ordinary poppet-type relief valve on the maket (nominal flow rate; 30 lt/min) is remodeled to meet the requirements.   Figure 9 illustrates the built-up experimental setup.   Figure 10 also shows the top-view geometry of an oil flow path in a poppet valve.   The poppet has a conical surfcae with a 35° taper, a rod and a piston in line.   The piston is held by a guide bore in the poppet seat, and the clearance between the poppet and the seat edge forms a restrictor.

As seen in Fig. 9, the poppet is pierced by two rods at both ends so that the clearance can be fixed at any position.   Accordingly, the poppet displacement is read by a dial gage outside of the valve via the thrust rod on the piston side.   Then, a steady flow of Turbine Oil 140♯ is given in such a direction as is indicated in Fig. 10.   After the poppet is fixed, semiconductor transducers measure the pre-
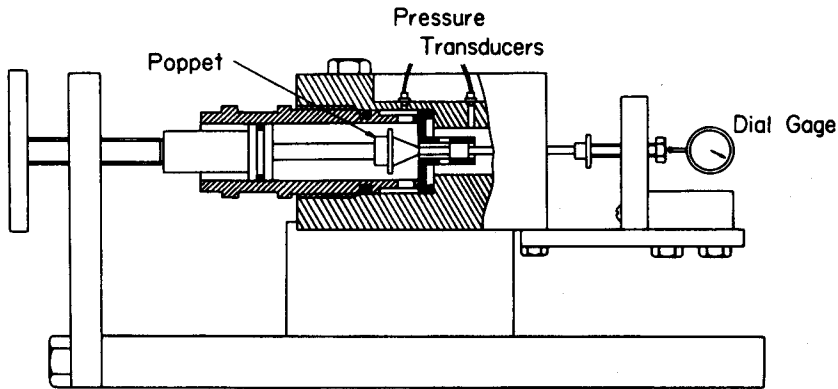
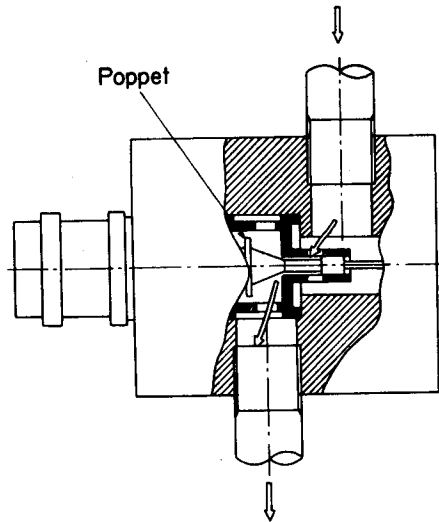Fig. 9. Experimental setup for poppet valve flow.

Fig. 10. Topviewed poppet valve geometry.

ssures at the upstream and downstream points across the restrictor, which are shown in Fig. 9. A scale weighs the flow rate at the outlet of the dischrage line in combination with a universal counter. Moreover, thermistors monitor the oil temperatures in the supply and discharge lines, and a water-type oil cooler helps to keep them as constant as possible all through the run.

3.2 Static measurements of opening area-loss relations

The poppet is fixed at 12 different positions. At each position, 15 to 20 sets of the pressure drop and flow rate data are obtained. When plotting those data for the same poppet position on a Δp—q diagram, we have the circles in Fig. 11, for example. In this figure, X means the axial displacement of the poppet, as is
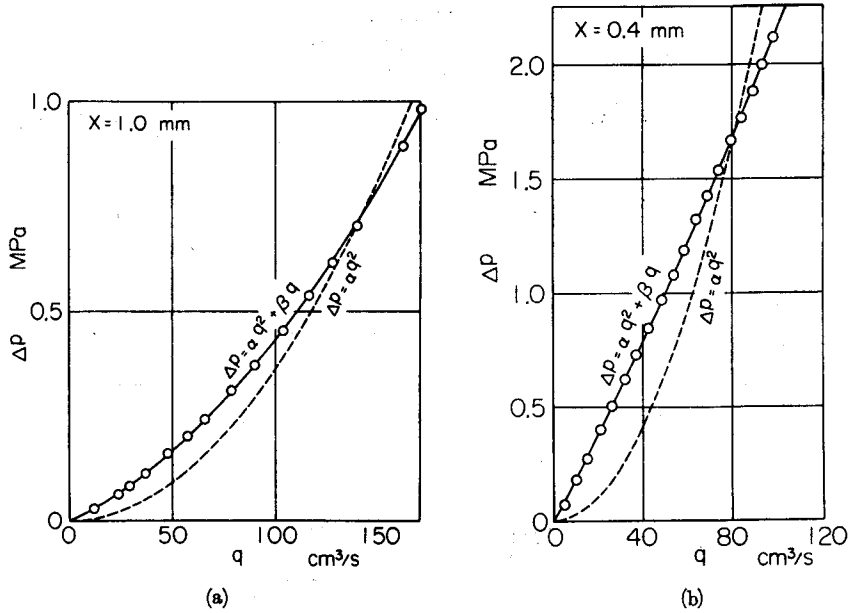
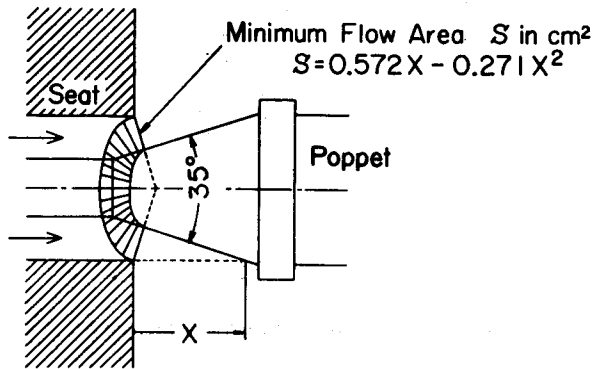Fig. 11.   Examples of $\Delta p - q$ relations for fixed poppet.

Fig. 12.   Definition of poppet opening area.

also illustrated in Fig. 12.   Supposing that these data points are predicted by the equation

$$\Delta p = \alpha q^2 \tag{5}$$

which is a simplified variation of Eq. (1), the least mean square method helps find α, shown by the broken curves in Fig. 11.   If the linear loss term is added to the right-hand side of Eq. (5) as

$$\Delta p = \alpha q^2 + \beta q \tag{6}$$

the same method is shown by the solid curves. Obviously, not Eq. (5) but Eq. (6) well represents the experimental results. It follows from these examples that when a poppet-type restrictor is used in an oil line, a high viscosity of oil causes a considerable linear loss beyond the usual non-linear loss.

It must be remembered here that both pressure holes are located some distance apart, with a complicated channel in between, except the restrictor as seen in Fig. 9. It means that the above-obtained total pressure drops necessarily include the channel losses and the kinetic energy difference between the two measuring sections. Hence, we next estimate the net pressure loss created by the poppet-seat restrictor alone.

The poppet is fixed in such a way that its conical surface is completely outside the seat hole. Thus, the displacement of the poppet no longer causes the raea of the restrictor mouth to vary. Conducting a similar measurement, we have the following empiric loss equation

$$\Delta p'' = \alpha'' q^2 + \beta'' q \tag{7}$$

where
$$\left. \begin{array}{l} \alpha'' = 2.75 \times 10^{-3} \quad \text{KPa}/(\text{cm}^3/\text{s})^2 \\ \beta'' = 0.296 \quad \text{KPa}/(\text{cm}^3/\text{s}) \end{array} \right\} \tag{8}$$

The pressure loss $\Delta p''$ is regarded as being brought about by the complicated channel geometry between the two detecting points, except the poppet-seat clearance. Therefore, subtracting $\Delta p''$ evaluated by Eq. (7) from the preceding Δp data, we obtain the net pressure loss $\Delta p'$.

A similar expression

$$\Delta p' = \alpha' q^2 + \beta' q \tag{9}$$

naturally well represents the newly-obtained $\Delta p' - q$ relations, and the least mean squre method is available again for evaluating α' and β'.

We next define the opening area S of the restrictor as follows. That is, imagine a cone the base of which is identical with the seat mouth, and which is orthogonal with the conical surface of the poppet, as illustrated in Fig. 12. Then, that part of its surface within the flow space represents the minimum cross section, and is assigned to S.

Plotting the evaluated values of α' and β' versus the reciprocal of the opening area, i.e., $1/S$, we have the circles in Fig. 13. The general figures data points form in Fig. 13 give rise to the tought that both α' and β' might be proportional to $(1/S)^2$. Evaluating those proportion constants by the least mean square method, we have the relations
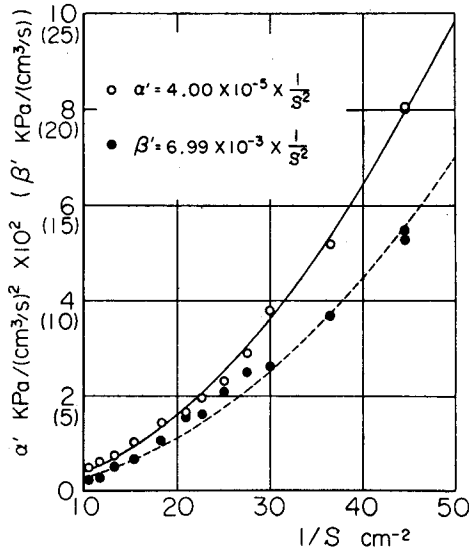
Fig. 13.   Dependencies of non-linear and linear loss
           coefficients on opening area for poppet-
           seat constriction.

$$\left.\begin{array}{l} \alpha' = 4.00 \times 10^{-5} \times \dfrac{1}{S^2} \quad (\mathrm{KPa}/(\mathrm{cm^3/s})^2) \\[4mm] \beta' = 6.99 \times 10^{-3} \times \dfrac{1}{S^2} \quad (\mathrm{KPa}/(\mathrm{cm^3/s})) \end{array}\right\} \tag{10}$$

which are shown by the curves in Fig. 13.   Presumably because the linear loss is more susceptible to the change of oil temperature, the solid circles for β' are rather scattered around the simulated curve.   Nonetheless, both curves seem to successfully represent the tendencies of the experimental results.   Hence, it can be concluded that α' and β' are both in inverse proportion to the square of S.

We reinforce this conclusion from another aspect.   That is, the net pressure losses $\varDelta p'$ required to create the same flow rate are calculated by Eq. (9) for various poppet displacements.   Plotting the results versus S on the abscissa, we have the circles in Fig. 14.   Circles of the same kind correspond to the same flow rate.   As known from Fig. 11, Eq. (9) predicts $\varDelta p'$ so accurately that the calculated values are practically regarded as being experimental.   On the other hand, substituting Eq. (10) into Eq. (9) and evaluating the $\varDelta p' - S$ relation by

$$\varDelta p' = \frac{1}{S^2}(4.00 \times 10^{-5} q^2 + 6.99 \times 10^{-3} q) \tag{11}$$

we have the curves in Fig. 14.   The circles lie pretty close on the curves, which
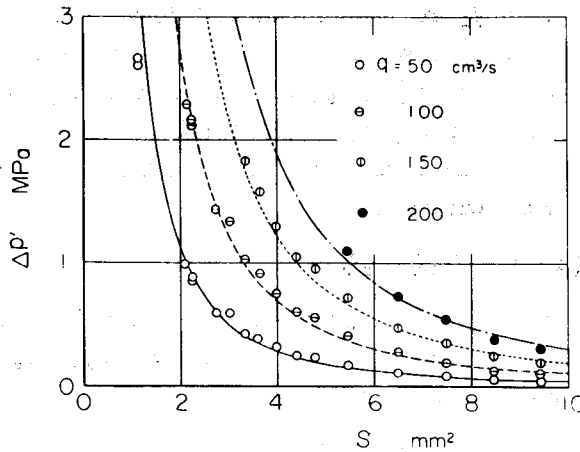
Fig. 14. Pressure drop-opening area relations with flow
rates as parameters for poppet-seat constriction.

backs up the validity of the above estimation of Eq. (10). It should be noticed
here that the flow rate is no more proportional to the opening area when a poppet-
type restrictor is used in oil flows. In other words, oil system engineers should be
deliberate in relying on the classical hydraulic formula Eq. (1) in the designing.
Equation (11) also suggests that a poppet valve is simulated by a circular orifice with
some thickness. If β' is estimated as the Poiseuille loss coefficient of the equiva-
lent orifice with a cross-sectional area S, we have its length as long as 2.20 cm.
Conceivably, this linear loss is brought about in the boundary layer developed
close to the conical surface of the poppet. Therefore, it is not too far from the
truth to imagine that the ratio of β' to $1/S^2$ in Eq. (10) is proportional to the oil
viscosity, which possibly has less influence on that for α'.

3.3 Performance as a relief valve

We are now concerned about how well the performance of the poppet valve
is predicted on the basis of Eq. (11), when it is ordinarily used as a pressure con-
trol device. The thrusting rod on the downstream side is replaced by a spring,
and a differential transformer measures the poppet displacement in place of the
dial gage.

The performance of this relief valve is dominated by the equilibrium condition
of forces exerting on the poppet, the pressure-flow rate characteristics of the dis-
charge line and the characteristics of the poppet restrictor. First, we take an
expedient way of estimating the poppet equilibrium, avoiding the troublesome
procedure of reckoning all kinds of forces acting on the poppet. That is, the
imbalance of the static pressures acting all over the poppet is simply estimated as

$p_1S_1-p_2S_2$, where p_1 and p_2 are the upstream and downstream detected pressures, and S_1 and S_2 are the effective cross-sectional areas on which they act. The spring thrust is expressed as $K(X+X_0)$, where K is the spring constant and X_0 is the initial compression of the spring. All other forces, which are caused by the flow around the poppet, are en bloc assigned to the 'fluid force' F_0. Finally, the equilibrium condition is written as

$$F_0+K(X+X_0)-(p_1S_1-p_2S_2) = 0 \qquad (12)$$

It is usually difficult to estimate F_0 separately, and also difficult to measure the preload KX_0. Hence, we try to find the dependency of F_0+KX_0 on the flow rate by measuring the right-hand side values of

$$F_0+KX_0 = -KX+(p_1S_1-p_2S_2) \qquad (13)$$

Figure 15 illustrates the results. Circles of the same kind belong to the same spring preload, and the dotted lines indicate their mean values.

The larger the preload is, the more scattered are the data points. Although it is conceivable that F_0 increases as the flow rate increases, Fig. 15 shows no distinct tendencies in this regard. Thus, for expedience' sake, we assume that F_0+KX_0 is independent of the flow rate, and given by the average value in Fig. 15.

Next, we require the pressure-flow rate relation in the discharge line. Since the discharge line of the present experimental setup does not include any
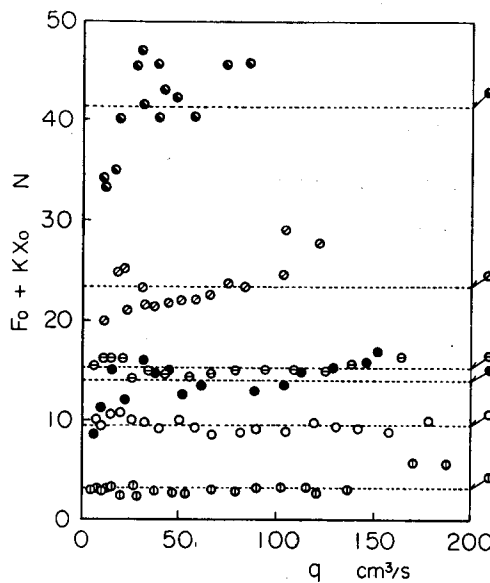

Fig. 15.   Estimation of fluid force.

nonlinear element, the pressure-flow rate relation at the downstream measuring section is expected to be given by

$$p_2 = C\nu q \tag{14}$$

where ν is the kinematic viscosity of the oil and C is the constant of proportion. Now, we seek such p_2 data as their corresponding temperature data stay within a 0.5°C difference. Plotting two examples of them on a p_2-q diagram, we have the circles in Fig. 16. With these data, the constant C is found to be 1.04 KPa·s²/cm² by the least mean square method. The lines in Fig. 16 are calculated by Eq. (14) with this value of C and the average values of ν.
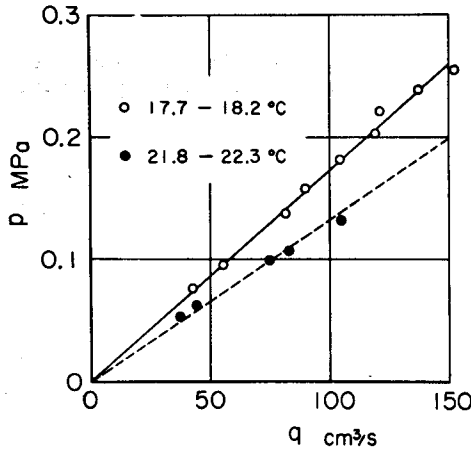

Fig. 16. p_2-q relation at downstream measuring
section.

The opening area S of the poppet-seat clearance is related to the poppet displacement X by

$$S = 5.72X - 0.271X^2 \qquad (S \text{ in } \mathrm{mm}^2,\ X \text{ in } \mathrm{mm}) \tag{15}$$

as written in Fig. 12. In order to simplify the calculation, we further linearize Eq. (15) as

$$S = 5.72X \tag{16}$$

Figure 17 demonstrates the deviation introduced by this approximation. The solid and broken lines are shown in Eq. (15) and Eq. (16), respectively.

To sum up, the characteristic equation for the poppet restrictor

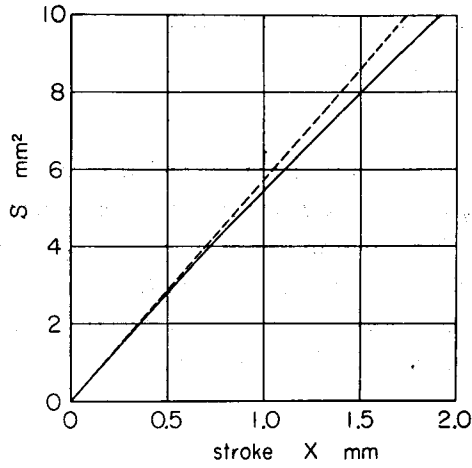$$p_1 - p_2 - (\alpha'' q^2 + \beta'' q) = (1/S^2)(\alpha' q^2 + \beta' q) \tag{17}$$

Fig. 17.   Theoretical relation between opening area and
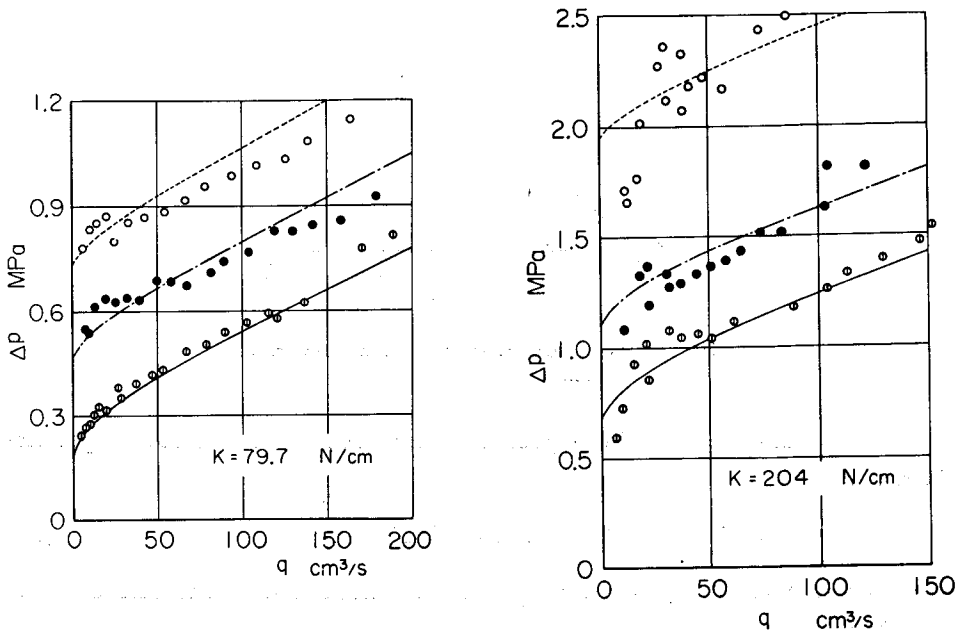poppet displacement and its approximation.

Fig. 18.   Poppet valve performances as pressure regulator.

and Eqs. (13), (14) and (16) are available for predicting the performcane of the
valve acting as a pressure regulator.   Measured pressure drop-flow rate relations
are compare with their predicted values in Fig. 18.   Here, two kinds of springs
are used, and three kinds of initial compression are given in each case.   Although
the poppet valve performances are roughly predicted, the experimental values are

too scattered to give any definite conclusion. This result suggests that it is more difficult than expected to precisely know the movement and force balance of the poppet when the valve is ordinarily acting.

4. Conclusions

Steady-state oil flows through constrictions like orifices and nozzles are experimentally investigated. The pressure loss and recovery in an orifice-in-a-pipe flow and the characteristics of a variable-area restrictor are our present concerns. A few findings cast some doubts on the conventional ideas about constriction flows in hydraulics. They are as follows:

(1) In a jet flow downstream from an orifice in a pipe, the pressure once drops a little and then makes a recovery. However, this behavior suddenly becomes unobservable when the Reynolds number falls below a certain critical value.

(2) The conventional view about the convergent flow upstream from an orifice is that the pressure on a pipe wall slightly increases toward the orifice wall in its vicinity. In fact, on the contrary, the pressure begins to decrease from a rather distant section upstream from the orifice. This peculiar phenomenon becomes more distinct as the Reynolds number becomes larger.

(3) Beyond the ordinary non-linear loss αq^2, a poppet-type restrictor produces the linear loss βq for oil flows. These coefficients α and β have proved to be in inverse proportion to the square of the opening area of the poppet-seat clearance. It follows that the flow rate is no more proportional to the opening area than expected.

References

1) H. P. Grace and C. E. Lapple; Trans. ASME; **73**, 639 (1951)
2) Y. Nakayama; Trans. JSME (in Japanese); **26**, 1485 (1960)
3) K. Komiya and K. Nagashio; Trans. SICE (in Japanese); **4**, 135 (1968)
4) H. S. Bean; Trans. ASME; **93**, 97 (1971)
5) B. Fujimoto; 'Hydraulics' (in Japanese); Yokendo Co. Ltd., (1963)